Carbonaceous composite materials from calcination of azo dye-adsorbed layered doubled hydroxide with enhanced photocatalytic efficiency for removal of Ibuprofen in water

Xiaolin Shen
Tongji University
ZHU Zhiliang (zzl@tongji.edu.cn)
Tongji University https://orcid.org/0000-0002-2516-1033
Hua Zhang
Tongji University
Guanglan Di
Tongji University
Ting Chen
Tongji University
Yanling Qiu
Tongji University
Daqiang Yin
Tongji University

Research

Keywords: layered double hydroxide, carbonaceous material, photodegradation, Ibuprofen, spent adsorbent reuse

Posted Date: December 10th, 2019

DOI: https://doi.org/10.21203/rs.2.18461/v1

Abstract

Background: The discard of used adsorbents may pose a great threat to human health and ecological environment. This work herein reported a facile and feasible method, with aims of (i) reusing the calcined layered double hydroxide (CLDH) adsorbent after azo dye adsorption, and (ii) being further used as a photocatalyst to enhance the degradation of typical pharmaceuticals. Calcination under inner gas flow has been utilized to carbonize adsorbed azo dye and a kind of novel carbonaceous CLDH composite material (CM-CLDH) was synthesized. This fabricated material was used as a catalyst for Ibuprofen removal in water samples under simulated sunlight irradiation.

Results: According to our experimental results, combination of carbonaceous material with CLDH showed an enhanced photocatalytic performance compared to original CLDH materials. More than 90% of Ibuprofen could be removed in less than 180 min. Photoluminescent spectra and transient photocurrent examination confirmed that suppressed recombination of photo-induced electrons and holes led to higher photocatalytic activities. Furthermore, conduct band potential (E CB) of the CM-CLDH became lower (-1.31 V), manifesting higher oxidation ability of accumulated electrons, leading to better photocatalytic activity. Under experimental conditions, the removal efficiency of Ibuprofen by CM-CLDH composite kept above 90% during five cycles.

Conclusion: Calcination under inner gas flow can transform organic pollutant-adsorbed CLDH to CM-CLDH composite with higher photocatalytic performance. A feasible way to reuse spent LDH adsorbents was proposed, which is benefit to reduce second pollution of spent adsorbents in environment.

1. Background

Azo dyes draw enormous attention for causing mutation and carcinoma through aromatic amines[1], and they are likely to trigger foul smell, eutrophication, decrease of dissolved oxygen amount when released into natural water, posing a threat to humans and aquatic ecosystem[2 – 3]. Adsorption[4], electrocatalysis[5] and photocatalysis[6] have been applied to deal with azo dye wastewater, among them, adsorption is preferred for its low cost, simple operation, high removal efficiency and reusability[7 – 8].

Layered double hydroxide (LDH) is a kind of hydrotalcite-like compounds, denoted as $[M_{(1-x)}^{2+}M_x^{3+}(OH)_2]_{layer}[A_{x/n}^{n-}\cdot zH_2O]_{interlayer}$, where M^{2+}, M^{3+} and A^{n-} represent divalent, trivalent metal cations and interlayer anions, respectively[4]. LDHs have been regarded as a kind of effective adsorbents attributing to their tunable charge densities and large specific surface areas[8], the interlayer anions can exchange with anions from contaminants[9], and large specific surface areas can provide with sufficient adsorption sites and reactive hydroxy for ligand exchange[10]. When calcined at moderate temperatures (400–500 °C), LDH's layered structure will collapse owing to interlayer anions' decomposition and release of interlayer water. Normally, calcined LDH (CLDH) exhibits favorable adsorption capacity and efficiency due to larger

specific surface areas and lamellar structure's reconstruction, researchers regard it as a kind of promising adsorbent for azo dye treatment[11 – 12].

After adsorption of anions from wastewater, treatment of spent LDHs becomes a tough challenge. Normal landfilling or piling up may result in foul smell, contamination of soil and underground water by leachate[13]. According to limited research consequences, after adsorption, Laipan et al. fabricated carbon-LDH composites via calcination under inert gas flow. The resulting material was efficient for Cr(VI) reduction[13], and it would be converted to metal ions and porous carbon through pickling. Metal ions were utilized for LDH synthesis once again, and porous structure was promising for toluene adsorption[14]. Nevertheless, researches related to using combination of organic pollutant-based carbonaceous material and LDH for photocatalysis are still limited. As mentioned in former research articles, addition of carbon-based materials like fullerence, graphene oxide (GO) and reduced graphene oxide (rGO) could promote LDH's photocatalytic efficiency. Further study pointed out that combination of LDHs and carbon-based materials would hamper recombination of photo-induced charges and aggregation of LDH layered structures[15 – 16]. Ju et al. fabricated fullerence/ZnAlTi-LDO composites, unique electronic properties allowed fullerence to act as an ideal electron acceptor to maintain effective separation of photo-induced electrons and holes[17]. GO and rGO own long-range π-π conjugations, remarkable electron mobility and specific surface area[16, 18–19], Zhu et al. pointed out that the electron mediator rGO in rGO/ZnFe-CLDH composite was enabled to improve the migration of electron from conduct band of ZnO to value band of $ZnFe_2O_4$, and Ni et al. argued that high work function of rGO caused movement of electron from value band of LDH to the surface of rGO[19], the aforementioned behavior succeeded in suppressing the recombination of photogenerated charge carriers and leading to an improved photocatalytic efficiency[18]. Apart from graphene-like materials, Mohamed et al. found that union of LDHs and polymer could also boost photocatalytic performance[20], polypyrrole (Ppy) nanofiber was able to provide larger specific surface area and decrease band gap of pristine LDH, which suggested lower energy consumption during producing single electron or hole, together with light-adsorption of wider wavelength range[21 – 22]. As a member of conjugated organic polymer, Ppy's conjugated P-electronic structure led to fast separation efficiency of photo-generated charge carrier, more electrons and holes could move to the surface then reacted to generate radicals. Though these mentioned materials facilitate certain photocatalytic performance, high price and relatively complex preparation process still restrict their applications.

To overcome the above deficiencies and make use of advantages of LDH materials, fabricating carbonaceous material and LDH composites (CM-CLDH) derived from spent LDH may reduce the cost of functional materials, avoid secondly environmental pollution from the abandoned adsorbents, and achieve recycling utilization of materials. Therefore, in this work, we focused on preparing carbonaceous functional composite material-CLDH (CM-CLDH) from azo dye adsorbed CLDH materials through calcination under inert gas protection. Typical azo food colorant amaranth (AM) was selected as dye pollutant and carbon source, calcined CLDH was chosen as adsorbent. First, adsorption was conducted by CLDH in amaranth solution. Second, spent CLDH was calcined under different temperature under nitrogen protection to obtain a series of CM-CLDHs. Third, the synthesized CM-CLDHs material was used

as a photocatalyst to study the removal performance of the Ibuprofen (IBF), one of the mass-produced and wide-distributed acesodyne[23] in water environment. The possible mechanisms of Ibuprofen removal were investigated and discussed. The stability and reusability of the composite CM-CLDHs as photocatalyst were also evaluated. This work can provide a feasible way to synthesize carbonaceous functional material by reusing spent LDH adsorbents, which is also benefit to reduce second pollution of spent adsorbents in environment.

2. Materials And Methods

2.1 Materials

All chemicals were purchased from chemical companies, no purification was operated on them during the experimental process. Zinc nitrate hexahydrate ($Zn(NO_3)_2·6H_2O$, AR grade), aluminum nitrate nonahydrate ($Al(NO_3)_3·9H_2O$, AR grade), sodium hydroxide (NaOH, AR grade), sodium carbonate (Na_2CO_3, AR grade), amaranth ($C_{20}H_{11}N_2Na_3O_{10}S_3$, FMP grade) and Ibuprofen ($C_{13}H_{18}O_2$, > 98%) were obtained from Sinopharm Chemical Reagent Co., Ltd (China). Lanthanum nitrate hexahydrate ($La(NO_3)_3·6H_2O$, AR grade) was purchased from Aladdin Co., Ltd (China). Ultrapure water was produced by a milli-Q device (18.2 MΩ·cm at 25 ℃).

2.2 Preparation of catalysts

2.2.1 Preparation of ZnAlLa-LDH

ZnAlLa-LDH was synthesized via co-precipitation method, 20 mmol $Zn(NO_3)_2·6H_2O$, 7.5 mmol $Al(NO_3)_3·9H_2O$ and 2.5 mmol $La(NO_3)_3·6H_2O$ were put into 50 mL ultrapure water to form stable solution through moderate stir. The mixture of metal nitrates was moved to a burette, then was dropwise added into a 300 mL beaker with 100 mL Na_2CO_3 solution (0.2 $mol·L^{-1}$), 1 $mol·L^{-1}$ NaOH was injected into the beaker via a peristaltic pump to keep solution's pH at 10 ± 0.1. The resulting slurry was stirred on magnetic stirrer for 1 hour before sent to drying oven for 24 hours' ageing. The obtained mixture was filtered by 0.45 μm filter membranes and washed by ultrapure water for three times. In the end, ZnAlLa-LDH was obtained after being dried at 80 ℃ overnight then ground into powder in mortar.

2.2.2 Preparation of ZnAlLa-CLDH

Aforementioned ZnAlLa-LDH was put in 20 mL crucible before sent to muffle furnace for calcination. Heating rate and heating time were controlled at 10 $℃·min^{-1}$ and 240 min. A series of CLDHs were synthesized with heating temperature controlled at 400, 500, 600 ℃, respectively. To distinguish, the obtained materials were successively noted as ZnAlLa-400CLDH, ZnAlLa-500CLDH, ZnAlLa-600CLDH.

2.2.3 Preparation of CM-CLDH catalyst

According to the screening result of adsorption performance, ZnAlLa-400CLDH presented highest adsorption efficiency among all the prepared ZnAlLa-CLDH materials. As for CM-CLDH fabrication,

ZnAlLa-400CLDH was added in 10, 20, 50, 100 mg/L amaranth with the dosage of 500 $mg \cdot L^{-1}$ to establish adsorption equilibrium. To be specific, in dye solution with concentration ranged from 10 to 100 mg/L, amaranth could be thoroughly adsorbed and removed by ZnAlLa-400CLDH. After suction filtration and washed by ultrapure water, the resulting precursor was sent to tube furnace for calcination at 400, 500, 600 ℃ under the protection of nitrogen (flow rate = 0.2 $L \cdot min^{-1}$), respectively. Meanwhile, the heating rate and heating time were controlled at 5 $℃ \cdot min^{-1}$ and 180 min. The final resulting product is named as CM-CLDH, which is a carbonaceous composite CLDH material.

2.3 Methods

2.3.1 Characterization

Detection of materials' Crystal phases were performed by a D-8 Advance X-ray diffractometer (Bruker-AXS, Germany) with Cu Ka radiation operated at 40 kV and 40 mA. Fourier transfer infrared (FTIR) spectra was obtained from Thermo Nicolet 5700 (Thermo Nicolet Corporation, USA). Microstructural characterization was carried out via scanning electron microscope (Nova nano SEM 450, FEI, Netherlands) and transmission electron microscope (JEM-2011, JEOL, Japan) equipped with energy-dispersive X-ray spectroscopy (EDX) mapping. X-ray photoelectron spectroscopy (XPS) plot was obtained from Thermo ESCALAB 250XI. Electron spin resonance (ESR) signals were investigated by ESR studio (Freiberg instruments Miniscope MS5000, Germany). Electrochemical properties were measured on electrochemical workstation (biological VSP-300, France).

2.3.2 Adsorption experiments

Batch adsorption experiments were carried out on magnetic stirring apparatus with reaction temperature controlled at 25 ± 5 ℃, 100 mL amaranth solution (concentration = 50 mg/L) was poured into 150 mL conical flask, sealed by aluminum foil. A certain amount of LDH/CLDHs (500 mg/L) were added into solution, then solution was stirred at 500 rpm for 6 hours. Syringe was used to collect sample at 20, 40, 60, 120, 180, 240, 300, 360 minutes after the start of adsorption experiments, the sample solution was filtered by 0.45 μm aqueous phase membrane before examined by UV-vis spectrophotometer (SOPTOP UV2400, China) at wavelength of 520 nm.

Experimental data was fitted by pseudo-first-order and pseudo-second-order kinetic models, two kinds of formulas were listed as follows:

$$\ln(q_e - q_t) = \ln q_e - k_1 t \quad (1)$$

$$\frac{t}{q_t} = \frac{1}{K_2 q_e^2} + \frac{t}{q_e} \quad (2)$$

where q_e and q_t successively represented adsorption capacity of the adsorbent at equilibrium and time t; K_1 (min^{-1}) and K_2 [g $(mg\ min)^{-1}$] represented adsorption rate constants of these two kinetic models.

In the meantime, adsorption isotherms were determined via batch equilibration method, with temperature set at 25 ± 5 ℃. 100 mL dye solution was added into each beaker, concentration of amaranth ranged from 10 to 1000 mg/L, dosage of adsorbents was 500 mg/L. After stirred on magnetic stirrer at 500 rpm for 16 hours, 2.5 mL of resulting solution was collected by syringe equipped with 0.45 μm aqueous phase membrane in sequence, then examined by UV-vis spectrophotometer at wavelength of 520 nm. Langmuir and Freundlich equation were chosen to assess adsorption behavior of amaranth onto ZnAlLa-400CLDH, the formulas were listed as follows:

$$\frac{C_e}{q_e} = \frac{C_e}{q_{max}} + \frac{1}{K_L q_{max}} \quad (3)$$

$$\log q_e = \log K_F + \frac{1}{n}\log C_e \quad (4)$$

where q_e (mg/g) was equilibrium adsorption capacity of amaranth onto ZnAlLa-400CLDH, q_{max} (mg/g) was the theoretical maximum monolayer sorption capacity, C_e (mg/L) was concentration of dye solution at equilibrium, K_L and K_F were Langmuir and Freundlich adsorption constants.

2.3.3 photocatalytic experiments

Photodegradation rate of IBF under simulated solar irradiation was applied to assess photocatalytic performance of prepared CM-CLDH composite materials. Simulated solar irradiation was generated by a 500 W xenon lamp (NBeT, China), light source wavelength was controlled by a 300 nm cut-off filter. Certain amount of IBF solution and catalysts were added into 100 mL quartz tube, mixed with magnetic stir bar. The quartz tubes were immobilized in a ring-like holder with 8 cm distance away from lamp, and the holder could rotate at a constant rate.

The mixture of IBF and catalyst CM-CLDH was magnetically stirred at dark for 30 minutes to minimize effect of adsorption, followed by light illumination for several hours. About 1 mL reaction solution samples were collected by syringe periodically, filtered by 0.22 μm water phase membrane to separate solid particles. The concentration of IBF in resulting solution was investigated by ultra-performance liquid chromatography equipped with photodiode array detector (Waters Acquity, USA).

3. Results And Discussions

3.1 Characterization

3.1.1 XRD analysis

Fig.1A displayed XRD patterns of prepared samples, including original ZnAlLa-LDH, ZnAlLa-CLDH, CLDH-AM and CM-CLDH (CLDH-AM was ZnAlLa-CLDH after adsorption in amaranth solution). As depicted in pattern, spiculate and symmetric peaks at 11.5°, 23.1°, 34.4° which were assigned to (003), (006) and

(009) planes indicated prepared materials' lamellar structure[24]. These aforementioned peaks, together with (105), (108), (110), (113) planes' peaks located at 38.9°, 44.6°, 59.9° and 61.2°, illustrated typical crystalline structure of LDH[25]. After calcination, these typical peaks disappeared, manifesting collapse of the original lamellar crystalline structure. With the increase of calcination temperature, peaks of obtained products became sharper, which may attribute to the formation of metal oxide[26]. After adsorption in amaranth solution, CLDH represented characteristic peaks of LDH again, which meant rehydration lamellar hydrotalcite-like structure reconstruction had been accomplished. Referred to former research, the main reason was LDH's intrinsic "memory effect" [27].

3.1.2 FTIR

As shown in Fig. 1B, peaks at around 3450 cm^{-1} were belonged to O-H stretching vibration of water on surface and intercalated into layered double hydroxide[28]. Intensity was weaker in calcined LDH, caused by water loss via calcination. The absorption band stood at 1367 cm^{-1} was connected with asymmetric stretching of interlayer carbonate[29]. Bands located at 500-1000 cm^{-1} region were related to metal-oxygen and metal-hydroxyl vibrations[30]. Asymmetric stretching vibration of S-O was observed at around 1200 cm^{-1}[31], and vibrations at region of 1100-1300 cm^{-1} of CLDH-AM were corresponding to SO_3^{2-} vibrations[29], manifesting amaranth was adsorbed by CLDH.

3.1.3 XPS

Fig. 1C and D expounded sectional high solution XPS spectra of CM-CLDH and used CM-CLDH (catalyst after photocatalysis). Full XPS spectra and high solution XPS spectra of residual elements were delivered in supporting information (Fig. S1). Signals of Zn 2p, Al 2p, La 3d, C 1s and O 1s could be detected in both samples. Zn 2p had two peaks at 1021.4 and 1044.6 eV, indicating Zn $2p_{1/2}$ and Zn $2p_{3/2}$ of Zn^{2+}, which could be assigned ZnO and $ZnAl_2O_4$[26]. Al 2p peak at 74.1 eV proved the existence of Al^{3+}[32].

Original La^{3+} peak was at 834.4 eV[33]. O 1s peak at 530.9 eV was assigned to metal-oxide chemical bonds[18]. C 1s peaks at 285.0 and 289.0 eV were attibuted to C-C and C=O species[18, 34]. After photocatalytic process, binding energy peaks had positive shifts, the probable cause was interaction between Ibuprofen anions and CM-CLDH during reaction, increase of electronegativity promoted attraction between extranuclear electrons and nuclear, which led to augment of binding energy[33].

3.1.4 Morphology

Fig. 2a and b demonstrated exterior structure of synthesized materials. ZnAlLa-CLDH got a sphere-like morphology, stacked by a large number of platelet-like units, which was in accordance with relevant research results[35]. After reaction in amaranth solution, the size of single nanoflakes became larger.

Furthermore, a part of nanoflakes exhibited rougher edges, together with some little particles appeared on their surface, these phenomena were caused by adsorption of amaranth.

As displayed in Fig. 2c and d, TEM patterns of CM-CLDH certified this material had a multi-layered structure. Moreover, interplanar spacing was measured by Digital Micrograph software, three obvious interplanar distances were severally 0.251, 0.193 and 0.243 nm, corresponding to (101), (102) planes of ZnO, and that of (311) planes attributing to $ZnAl_2O_4$. The selected area electron diffraction (SAED) pattern demonstrated through calcination, polycrystalline phase had been constructed in CM-CLDH[36], which could also be proved by XRD patterns.

Elemental mapping analysis had been conducted simultaneously, the results of Fig. 3 elucidated that zinc, aluminum, lanthanum, oxide and carbon were the main components of CM-CLDH. These five elements uniformly dispersed throughout sample, only a part of zinc and lanthanum accompanied with oxygen constructed sphere-like structure, which might relate to the formation of ZnO and La_2O_3.

3.1.5 Thermal analysis

Fig. S2 exhibited thermogravimetry curves of synthesized materials and amaranth. As for LDH, weight loss from 50 ℃ to 168 ℃ and 168 ℃ to 242 ℃ were related to evaporation of water absorbed on the crystalline surface and intercalated into layers successively[4]. The weight of water evaporated accounted for 17.6 % of the total weight of LDH. During 242 ℃ to 336 ℃, dehydroxylation and decomposition of some interlaminar carbonate led to 3.7 % weight loss. With continuous temperature rise from 336 ℃ to 800 ℃, residual carbonate decomposed and the lamellar structure collapsed[37].

Amaranth kept stable during 50 ℃ to 300 ℃, then a rapid weight loss could be spotted with temperature risen from 300 ℃ to 800 ℃. A great number of aromatic groups might provide amaranth with a prominent thermal stability. When temperature rose to a relevant high range, the aromatic structure triggered carbonation process, which could explain sharp decrease of weight loss[38]. The carbonaceous products remained stable, so there was still 51.9 % residue of amaranth left at 800 ℃.

Compared with pristine LDH, CLDH-AM suffered from less weight loss in the first step, indicating weaker interaction between LDH and water. In the end, total mass loss of the composite CLDH-AM material was 21.3 %, much less than LDH (33.05 %), demonstrating the intercalation of amaranth could improve thermal stability and hydrophobicity of LDH[14].

3.2 Amaranth adsorption experiments

As shown in Fig. 4a, CLDHs calcined at 400, 500, 600 ℃ showed obviously higher adsorption capacity of amaranth than LDH, driven by larger specific surface area and “memory effect” as mentioned previously.

No significant difference had been found on CLDHs' adsorption capacity and rate, calcination temperature had a negligible effect on amaranth adsorption in this experiment. All three adsorbents could reach adsorption equilibrium at 180 min, and ZnAlLa-400CLDH got a relevant higher reacion rate, so this material was chosen for follow-up experiments and characterizaions.

Table 1 Kinetic parameters for the adsorption of amaranth on ZnAlLa-400CLDH

Sample	$q_{e,exp}$ (mg/g)	Pseudo-first-order model			Pseudo-second-order model		
		$q_{e,cal}$ (mg/g)	k_1 (min^{-1})	R^2	$q_{e,cal}$ (mg/g)	k_2 (*10^{-4} g mg^{-1} min^{-1})	R^2
ZnAlLa-400CLDH	100	100.1	0.025	0.999	114.0	2.853	0.988

Table 2 Isotherm parameters of adsorption of amaranth onto ZnAlLa-400CLDH

Sample	Langmuir equation				Freundlich equation		
	q_{exp} (mg/g)	q_m (mg/g)	K_L (L/m4g)	R^2	n	K_F (L/g)	R^2
ZnAlLa-400CLDH	602.5	555.6	0.059	0.911	4.549	142.3	0.949

Adsorption kinetics and adsorption isotherms of amaranth on ZnAlLa-400CLDH was fitted by pseudo-first-order model and Freundlich isothem model, respectively. Pseudo-first-order model was proposed by Lagergren, in this model, adsorbate-diffusion via a boundary occurred in advance of adsorption[39]. Adsorbent owing heterogeneous surface is the basic assumption of Freundlich isotherm. In this empirical model, adosption was a heterogenetic process, interactions between adsorbates were taken into account[40]. Besides, the increase of uptake capacity would lead to exponential reduction in binding energy of surficial multilayers from adsorbed ions[41]. Hence, a large amount of amaranth molecules might be adsorbed on the surface of ZnAlLa-400CLDH stacks by stacks, which was in consonance with SEM images.

3.3 Photocatalysis experiments

After getting adsorption equilibrium of 50 mg/L amaranth, the composite material CLDH-AM were sent to tubular furnace for calcination, temperature was set at 400, 500 and 600°C, respectively. The resulting

materials were noted as 400CM-CLDH, 500CM-CLDH and 600CM-CLDH, then utilized as photocatalysts in Ibuprofen degradation experiments, detailed procedures were recorded in 2.5. Fig. 5 recorded data of photodegradation process, X axis represented time (min) and Y axis represented the ratio of sampled solution's concentration (C) and initial concentration (C_0). The consequence (Fig. 5a) inlucidated that when amount of carbon source was equal, composites calcined at 500 ℃ had a higher photodegradation efficiency.

To evaluate the effect of carbon source amount on photocatalytic efficiency, in the following step, ZnAlLa-400CLDH was stirred in amaranth solution (concentration controlled at 10, 20, 50, 100 respectively) overnight for amaranth thoroughly adsorbed by ZnAlLa-400CLDH. Then resulting composites were calcined at 500 ℃ under nitrogen flow. Samples were correspondingly noted as CM-CLDH10, CM-CLDH20, CM-CLDH50, CM-CLDH100. As displayed in Fig. 5b, with the decrease of adsorbed amaranth, the resulting catalysts exhibited higher working efficiency.

When compared with pristine CLDHs calcined at 400, 500 and 600 ℃, CM-CLDH10 still presented obvious advantages, curves of C/C_0 dropped rapidly especially in the first 60 minutes. Pseudo-first-order equation derived from Langmuir-Hinshelwood model was used to evaluate kinetics of photocatalytic process[42], the formula could be expressed as follows:

$$\ln(C_0/C) = k_{app} * t \quad (5)$$

where k_{app} represented the apparent pseudo-first-order rate constant, C_0 and C were pollutant concentration at the start and the end of reaction. Higher k_{app} value normally indicated faster photodegradation process of a catalyst, k_{app} of CM-CLDH10, pure ZnAlLa-CLDHs and their pseudo-first-order kinetic plots were shown in Fig. 5d. Obviously, CM-CLDH10 displayed the highest photodegradation rate. Additionally, in CM-CLDH10 systhem, it removed more than 90 % Ibuprofen with the least time comsumption, which could be regarded as the most effective catalysts in this work. Moreover, CM-CLDH10 was collected via suction filtration after photocatalysis, recycled sample was used in IBF photodegradation experiments for another four times to evaluate its recyclability and stability. As depicted in Fig. S3, after five runs, photodegradation efficiency of CM-CLDH10 descreased from 94.9 % to 89.7 %, indicating promising recyclability and stability of synthezised catalyst.

3.4 Photodegradation mechanisms

3.4.1 Effect of solution pH

Original pH of 5 mg/L Ibuprofen solution in this experiment was 5.90. Nitric acid and sodium hydroxide (0.5 mol/L) were injected by syringe to regulate pH of Ibuprofen at 3, 5, 7 and 9 (3.06, 4.96, 6.96, 9.05 in effect). Photodegradation efficiencies over CM-CLDH10 under these four pH conditions were provided by Fig. 6a. With the decrease of pH values, CM-CLDH10 presented higher photodegradation efficiency, at pH

= 3.06 more than 95 % of target comtaminant could be removed in 60 minutes, faster than that of other conditions. Interstingly, photodegradation rate gradually declined with the increase of pH value. On the basis of former researches, acidic solutions could promote photodegradation through acceleration of ·OH manufacture[42]. Moreover, H^+ would react with $\cdot O_2^-$ to generate $HO\cdot_2$, both $\cdot O_2^-$ and $HO\cdot_2$ had clear advantage in ring clevage of aromatic groups[43-44]. According to scavenger experiment, effect of ·OH could be neglected, so attack of $\cdot O_2^-$ and $HO\cdot_2$ on Ibuprofen's aromatic ring might be indispensible during photodegradation. On the other hand, with the increase of pH, holes' oxidation ability would diminish due to cathodic displacement happened on valence band position[42]. And too many OH^- could also form hydrogen oxidation film during photocatalytic process, which hampered efficiency of catalysts[17].

3.4.2 Radical species detection

Radical species (RS) (mainly hydroxyl radical (·OH) and superoxide radical ($\cdot O_2^-$)) and singlet oxygen ($^1O_2$) play a vital role in photodegradion on organic contaminants. RS scavengers like tertiery buthanol (BuOH), ethylenediaminetetraacetic acid disodium (EDTA-2Na), benzoquine (BQ), $K_2Cr_2O_7$ and L-histidine were added into reaction system respectively to probe ·OH, holes (h^+), $\cdot O_2^-$, electrons (e^-) and $^1O_2$. As depicted in Fig. 6b, involvement of L-histidine, $K_2Cr_2O_7$ and BQ distinctly hampered efficiency and rate of photodegradation, which reflected singlet oxygen, electron and superoxide radical were dominant radicals during photocatalytic process[45-47]. On the contrary, addition of EDTA-2Na and BuOH showed limited inhibiting effect, revealing photo-induced holes and hydroxyl radicals' attack on Ibuprofen was relatively weak[47-48].

Electronic spin resonance (ESR) test was also performed to investigate main radical species during photocatalytic process. As for hydroxyl radical and singlet oxygen, 5 mL water and 5 mg catalyst were added into quartz reacion dish, then severally injected 5 μL 5,5-Dimethyl-1-pyrroline N-oxide (DMPO) and 2,2,6,6-tetramethylpiperidine (TEMP) as spin-trapping agent. The resulting mixture was irradiated under a ultraviolet lamp for 5 minutes before being sampled in capillary tube for detection. Method for superoxide radical was similar, the only difference was 5 mL water being substituted by 5 mL DMSO (dimethyl sulfoxide).

As shown in Fig. 6c and d, both ZnAlLa-500CLDH and CM-CLDH10 exhibited characteristic peaks of DMPO-$\cdot O_2^-$ and TEMP-$^1O_2$ with intensity ratio of 1:1:1:1:1:1 and 1:1:1. And relative intensity of DMPO-$\cdot O_2^-$ was higher in CM-CLDH10, suggesting involvement of carbonaceous material might lead to improvement of photodegradation. Moveover, after ultraviolet irradiation for 5 minutes, only CM-CLDH10 generated sufficient ·OH to be captured by DMPO, this evidence also reflected that combination with carbonaceous material could make CLDH present higher radical productivity, which might promote its photocatalytic performance.

3.5 Photoelectronic property

Photoluminescence (PL) singal would be generated at the time of photo-induced electrons and holes' recombination[49], the higher intensity indicated lower separation efficiency of photo-generated carriers. With excitation wavelength set at 350 nm, PL signals of ZnAlLa-500CLDH and CM-CLDH10 were detected in the wavelength range of 365–600 nm (Fig. 7a). The consequence reflected that PL signal intensity of CM-CLDH10 was lower, manifesting better separation ability of photo-induced electrons and holes, which might be an important factor for better photocatalytic performance over CM-CLDH10. Photocurrent transient curves were obtained, the transient photocurrent responses of CM-CLDH10 was much higher than that of ZnAlLa-500CLDH, revealling carbonaceous material had a positive effect on separation of electrons and holes[50]. This conclusion was further proved by transient photocurrent response. As reflected in Fig. 7b, stronger intensity has been spotted on CM-CLDH10, which was triggered by higher separation efficiency of photo-induced h^+ and e^-[51].

Electrochemical impedance spectroscopy (EIS) curves were applied to assess electrochemical performances of synthesized materials. In this test, 1 $mol{\cdot}L^{-1}$ sodium hydroxide carbon rod and saturated calomel electrode were utilized as electrolyte, counter electrode and reference electrode.

Fig. 7c exhibited EIS plots of both catalysts, applied potential was 1.5 V (versus RHE) from 1000 kHz to 0.01 Hz in 1.0 $mol{\cdot}L^{-1}$ sodium hydroxide electrolyte. Much larger semicircle's radius in Nyquist plot was connected with worse charge transfer resistance[52]. On the basis of PL, photocurrent and EIS test, photo-induced electrons and holes were generated mainly by CLDH's MO_6 octahedra which shared Metal-Oxygen bonds[53], introduction of carbonaceous material could reduce recombination of photo-induced carriers. Nevertheless, its conductive activity was lower than pure metal or metal oxide, which might explain why photodegradation efficiency was falling down with the increase amount of carbonaceous material on ZnAlLa-CLDH.

3.6 Energy band structure

According to UV-vis/DRS spectra, with increase of adsorbed amaranth amount, UV absorbance spectrum of resulting calcination product shifted to longer wavelength region, which suggested combination of carbonaceous material improved light adsorption[54]. Kubelka-Munk method driven transformed reflectance spectras were attained to measure energy band (Eg) of ZnAlLa-500CLDH and CM-CLDH10[55], Eg values were 3.37 eV and 3.21 eV, involvement of carbonaceous material narrowed band gap, which could improve photocatalytic activity. Mott-Schottky plots via implementing Mott-Schottky measurement was applied to estimate conduction band potential (E_{CB}) of prepared materials (saturated calomel electrode as reference electrode, 0.2 M Na_2SO_4 as electrolyte, pH = 7). As shown in Fig. 8c and d, E_{CB} values of n-type ZnAlLa-500CLDH and CM-CLDH10 were -0.71 V and -1.27 V (V vs NHE), after

transformation from E (SCE) to E (NHE)[56]. As is known to all, Eg = E_{VB} – E_{CB}, calculated value of valence band potential (E_{VB}) were 2.66 V and 1.9 V.

According to aforementioned analysis, potential mechanism of photodegradation could be listed as follows:

CM-CLDH10 + hv → e^- + h^+ (6)

e^- + O_2 → $\bullet O_2^-$ (7)

H^+ + $\bullet O_2^-$ → $HO\bullet_2$ (8)

$\bullet O_2^-$ + h^+ → $^1O_2$ (9)

Ibuprofen + $\bullet O_2^-$ → photocatalytic product (10)

Ibuprofen + $HO\bullet_2$ → photocatalytic product (11)

Ibuprofen + $^1O_2$ → photocatalytic product (12)

4. Conclusion

In summary, this study proved that calcined LDH can effectively remove azo dye through “memory effect” driven adsorption. After calcination under nitrogen atmosphere, the resulting carbonaceous composite material exhibited higher photocatalytic activity, supported by Ibuprofen photodegradation experiment. PL and photocurrent plots confirmed that involvement of carbonaceous material can hamper recombination of photo-induced carriers. The composite catalyst could generate $\bullet O_2^-$, $^1O_2$ to oxidize Ibuprofen, in low pH range, generation of $HO\bullet_2$ would accelerate collapse of aromatic nucleus. This work has provided a strategy to reuse the spent adsorbent after treatment of organic pollutants for preparation of novel carbonaceous functional materials. It shows a potential to reduce second pollution of spent adsorbents in environment and to recycle adsorbent materials.

Abbreviations

CLDH:calcined layered double hydroxide; CM-CLDH:carbonaceous material-CLDH; AM:amaranth; IBF:Iburopfen; XRD:X-ray diffractometry; FTIR:Fourier transform infrared spectroscopy; SEM:scanning electron microscope; TEM:Transmission electron microscope; UPLC:ultra-performance liquid chromotography; PL:photoluminescence; EIS:electrochemical impedance spectroscopy; RS:radical species; DMPO:5,5-Dimethyl-1-pyrroline N-oxide; TEMP:2,2,6,6-tetramethylpiperidine; DMSO:dimethyl sulfoxide; BuOH:tertiary buthanol; BQ:benzoquinone; EDTA-2Na:ethylenediaminetetraacetic acid disodium;

Declarations

Ethics approval and consent to participate

Not applicable

Consent for publication

Not applicable

Availability for data and materials

All data generated or analysed during this study are included in this published article [and its supplementary information files].

Competing interests

The authors declare that they have no competing interests.

Funding

This work was supported by National Science and Technology Major Project of China (Grant No. 2017ZX07201005).

Authors' contributions

XS performed experiments, data analysis, and wrote the manuscript. ZZ gave the guidance to experiment design and made a detailed manuscript discussion and modification. TC and GD made contributions to some experiment designs. YQ and HZ gave guidance and support on instrumental analysis. DY gave substantial suggestions on experimental design.

Acknowlegement

Thanks to the funding support of Ministry of Science and Technology of China.

References

1. Zhang G, Ma Y (2013) Mechanistic and conformational studies on the interaction of food dye amaranth with human serum albumin by multispectroscopic methods. Food Chem 136(2): 442-449.
2. Barros W, Steter J, et al., (2016) Catalytic activity of Fe_3−xCu_xO_4 (0≤x≤0.25) nanoparticles for the degradation of Amaranth food dye by heterogeneous electro-Fenton process. Appl Cata B-Environ 180: 434-441.
3. Abdellaoui K, Pavlovic I, et al., (2017) A comparative study of the amaranth azo dye adsorption/desorption from aqueous solutions by layered double hydroxides. Appl Clay Sci 143: 142-

150.

4. Santos R, Tronto J, et al., (2017) Thermal decomposition and recovery properties of ZnAl–CO_3 layered double hydroxide for anionic dye adsorption: insight into the aggregative nucleation and growth mechanism of the LDH memory effect. J Mater Chem A 5(20): 9998-10009.
5. Zhang Y, He P, et al., (2019) Ti/PbO_2-Sm_2O_3 composite based electrode for highly efficient electrocatalytic degradation of alizarin yellow R. J Colloid Interf Sci 533: 750-761.
6. Nath I, Chakraborty J, et al., (2018) Engineered synthesis of hierarchical porous organic polymers for visible light and natural sunlight induced rapid degradation of azo, thiazine and fluorescein based dyes in a unique mechanistic pathway. Appl Cata B-Environ 227: 102-113.
7. Shan R, Yan L, et al., (2014) Magnetic Fe_3O_4/MgAl-LDH composite for effective removal of three red dyes from aqueous solution. Chem Eng J 252: 38-46.
8. Lei C, Pi M, et al., (2017) Organic dye removal from aqueous solutions by hierarchical calcined Ni-Fe layered double hydroxide: Isotherm, kinetic and mechanism studies. J Colloid Interf Sci 496: 158-166.
9. Lu H, Zhu Z, et al., (2015) Simultaneous removal of arsenate and antimonate in simulated and practical water samples by adsorption onto Zn/Fe layered double hydroxide. Chem Eng J 276: 365-375.
10. Cai J, Zhao X, et al., (2018) Enhanced fluoride removal by La-doped Li/Al layered double hydroxides. J Colloid Interf Sci 509: 353-359.
11. Lei C, Zhu X, et al., (2017) Superb adsorption capacity of hierarchical calcined Ni/Mg/Al layered double hydroxides for Congo red and Cr(VI) ions. J Hazard Mater 321: 801-811.
12. Zaghouane-Boudiaf H, Boutahala M, et al., (2012) Removal of methyl orange from aqueous solution by uncalcined and calcined MgNiAl layered double hydroxides (LDHs). Chem Eng J 187: 142-149.
13. Laipan M, Fu H, et al., (2017) Converting Spent Cu/Fe Layered Double Hydroxide into Cr(VI) Reductant and Porous Carbon Material. Sci Rep-UK 7(1): 7277.
14. Laipan M, Zhu R, et al., (2015) From spent Mg/Al layered double hydroxide to porous carbon materials. J Hazard Mater 300: 572-580.
15. Daud M, Kamal M, et al., (2016) Graphene/layered double hydroxides nanocomposites: A review of recent progress in synthesis and applications. Carbon 104: 241-252.
16. Liang J, Wei Y, et al., (2019) Constructing high-efficiency photocatalyst for degrading ciprofloxacin: Three-dimensional visible light driven graphene based NiAlFe LDH. J Colloid Interf Sci 540: 237-246.
17. Ju L, Wu P, et al., (2017) Synthesis and characterization of Fullerene modified ZnAlTi-LDO in photo-degradation of Bisphenol A under simulated visible light irradiation. Environ Pollut 228: 234-244.
18. Zhu J, Zhu Z, et al., (2018) Calcined layered double hydroxides/reduced graphene oxide composites with improved photocatalytic degradation of paracetamol and efficient oxidation-adsorption of As(III). Appl Catal B-Environ 225: 550-562.
19. Ni J, Xue J, et al., (2017) Construction of magnetically separable NiAl LDH/Fe3O4-RGO nanocomposites with enhanced photocatalytic performance under visible light. Phys Chem Chem

Phys 20(1): 414.

20. Mohamed F, Abukhadra M, et al., (2018) Removal of safranin dye from water using polypyrrole nanofiber/Zn-Fe layered double hydroxide nanocomposite (Ppy NF/Zn-Fe LDH) of enhanced adsorption and photocatalytic properties. Sci Total Environ 640-641: 352-363.
21. Di G, Zhu Z, et al., (2017) Simultaneous removal of several pharmaceuticals and arsenic on Zn-Fe mixed metal oxides: Combination of photocatalysis and adsorption. Chem Eng J 328: 141-151.
22. Shaban M, Abukhadra M, et al., (2018) Recycling of glass in synthesis of MCM-48 mesoporous silica as catalyst support for Ni_2O_3 photocatalyst for Congo red dye removal. Clean Technol Envir 20(1): 13-28.
23. Vebber M, Aguzzoli C, et al., (2019) Self-assembled thin films of PAA/PAH/TiO_2 for the photooxidation of ibuprofen. Part II: Characterization, sensitization, kinetics and reutilization. Chem Eng J 361: 1487-1496.
24. Tzompantzi, Carrera Y, et al., (2013) ZnO–Al_2O_3–La_2O_3 layered double hydroxides as catalysts precursors for the esterification of oleic acid fatty grass at low temperature. Catal Today 212: 164-168.
25. Busetto C, Del Piero G, et al., (1984) Catalysts for low-temperature methanol synthesis. Preparation of Cu-Zn-Al mixed oxides via hydrotalcite-like precursors. J Catal 85(1): 260-266.
26. Zhu J, Zhu Z, et al., (2016) Enhanced photocatalytic activity of Ce-doped Zn-Al multi-metal oxide composites derived from layered double hydroxide precursors. J Colloid Interf Sci 481: 144-157.
27. Zhao Q, Tian S, et al., (2015) Novel HCN sorbents based on layered double hydroxides: Sorption mechanism and performance. J Hazard Mater 285: 250-258.
28. Lupa L, Cocheci L, et al., (2018) Phenol adsorption using Aliquat 336 functionalized Zn-Al layered double hydroxide. Sep Purif Technol 196: 82-95.
29. Guo Y, Zhu Z, et al., (2013) Enhanced adsorption of acid brown 14 dye on calcined Mg/Fe layered double hydroxide with memory effect. Chem Eng J 219: 69-77.
30. José dos Reis M, Silvério F, et al., (2004) Effects of pH, temperature, and ionic strength on adsorption of sodium dodecylbenzenesulfonate into Mg–Al–CO_3 layered double hydroxides. J Phys Chem Solids 65(2): 487-492.
31. Zhao Y, Chen G, et al., (2015) Defect-Rich Ultrathin ZnAl-Layered Double Hydroxide Nanosheets for Efficient Photoreduction of CO_2 to CO with Water. Adv Mater 27(47): 7824-7831.
32. Seo Y, Choi T, et al., (2015) Enhancement of stability of aqueous suspension of alumina nanoparticles by femtosecond laser irradiation. J Appl Phys 118(11): 114906.
33. Li H, Xin C, et al., (2015) Direct carbonylation of glycerol with CO_2 to glycerol carbonate over Zn/Al/La/X (X=F, Cl, Br) catalysts: The influence of the interlayer anion. J Mol Catal A-Chem 402: 71-78.
34. Huang Z, Wang T, et al., (2019) Coagulation treatment of swine wastewater by the method of in-situ forming layered double hydroxides and sludge recycling for preparation of biochar composite

catalyst. Chem Eng J 369: 784-792.

35. Gao Z, Sasaki K, et al., (2018) Structural memory effect of Mg-Al and Zn-Al layered double hydroxides in the presence of different natural humic acids: Process and mechanism. Langmuir 34(19).
36. Wang R, Wen T, et al., (2014) Highly efficient removal of humic acid from aqueous solutions by Mg/Al layered double hydroxides–Fe_3O_4 nanocomposites. RSC Adv 4(42): 21802-21809.
37. Gasser M, Mohsen H, et al., (2008) Humic acid adsorption onto Mg/Fe layered double hydroxide. Colloid Surface A 331(3): 195-201.
38. Kutlu B, Leuteritz A, et al., (2014) Stabilization of polypropylene using dye modified layered double hydroxides. Polym Degrad Stabil 102: 9-14.
39. Ahmed I, Gasser M (2012) Adsorption study of anionic reactive dye from aqueous solution to Mg–Fe–CO_3 layered double hydroxide (LDH). Appl Surf Sci 259: 650-656.
40. Wang X, Jiang C, et al., (2018) Carbon composite lignin-based adsorbents for the adsorption of dyes. Chemosphere 206: 587-596.
41. Bagherifam S, Komarneni S, et al., (2014) Highly selective removal of nitrate and perchlorate by organoclay. Appl Clay Sci 95: 126-132.
42. Wang X, Wu P, et al., (2014) Solar photocatalytic degradation of methylene blue by mixed metal oxide catalysts derived from ZnAlTi layered double hydroxides. Appl Clay Sci 95: 95-103.
43. Ng J, Wang X, et al., (2011) One-pot hydrothermal synthesis of a hierarchical nanofungus-like anatase TiO2 thin film for photocatalytic oxidation of bisphenol A. Appl Catal B-Environ 110: 260-272.
44. Zhang L, Wong K, et al., (2010) Effective Photocatalytic Disinfection of E. coli K-12 Using AgBr–Ag–Bi_2WO_6 Nanojunction System Irradiated by Visible Light: The Role of Diffusing Hydroxyl Radicals. Environ Sci Technol 44(4): 1392-1398.
45. Yun E, Lee J, et al., (2018) Identifying the Nonradical Mechanism in the Peroxymonosulfate Activation Process: Singlet Oxygenation Versus Mediated Electron Transfer. Environ Sci Technol 52(12): 7032-7042.
46. Xie X, Zhang N, et al., (2018) $Ti_3C_2T_x$ MXene as a Janus cocatalyst for concurrent promoted photoactivity and inhibited photocorrosion. Appl Catal B-Environ 237: 43-49.
47. Jo W, Kim Y, et al., (2018) Hierarchical flower-like NiAl-layered double hydroxide microspheres encapsulated with black Cu-doped TiO_2 nanoparticles: Highly efficient visible-light-driven composite photocatalysts for environmental remediation. J Hazard Mater 357: 19-29.
48. Najafian H, Manteghi F, et al., (2019) Fabrication of nanocomposite photocatalyst $CuBi_2O_4$/Bi_3ClO_4 for removal of acid brown 14 as water pollutant under visible light irradiation. J Hazard Mater 361: 210-220.
49. Liu X, Ma C, et al., (2013) Hydrothermal Synthesis of CdSe Quantum Dots and Their Photocatalytic Activity on Degradation of Cefalexin. Ind Eng Chem Res 52(43): 15015-15023.

50. Jo W, Kim Y, et al., (2018) Hierarchical flower-like NiAl-layered double hydroxide microspheres encapsulated with black Cu-doped TiO_2 nanoparticles: Highly efficient visible-light-driven composite photocatalysts for environmental remediation. J Hazard Mater 357: 19-29.
51. Zang S, Zhang G, et al., (2019) Enhancement of photocatalytic H_2 evolution on pyrene-based polymer promoted by MoS_2 and visible light. Appl Catal B-Environ 251: 102-111.
52. Chen F, Yang Q, et al., (2017) Hierarchical assembly of graphene-bridged Ag_3PO_4/Ag/$BiVO_4$ (040) Z-scheme photocatalyst: An efficient, sustainable and heterogeneous catalyst with enhanced visible-light photoactivity towards tetracycline degradation under visible light irradiation. Appl Catal B-Environ 200: 330-342.
53. Chen Y, Rui K, et al., (2019) Recent Progress on Nickel-Based Oxide/(Oxy)Hydroxide Electrocatalysts for the Oxygen Evolution Reaction. Chem-Eur J 25(3): 703-713.
54. Cho S, Lee K (2011) Formation of zinc aluminum mixed metal oxide nanostructures. J Alloy Compd 509(35): 8770-8778.
55. Ng J, Xu S, et al., (2010) Hybridized Nanowires and Cubes: A Novel Architecture of a Heterojunctioned TiO_2/$SrTiO_3$ Thin Film for Efficient Water Splitting. Adv Funct Mater 20(24): 4287-4294.
56. Zheng J, Lei Z (2018) Incorporation of CoO nanoparticles in 3D marigold flower-like hierarchical architecture $MnCo_2O_4$ for highly boosting solar light photo-oxidation and reduction ability. Appl Catal B-Environ 237: 1-8.

Figures

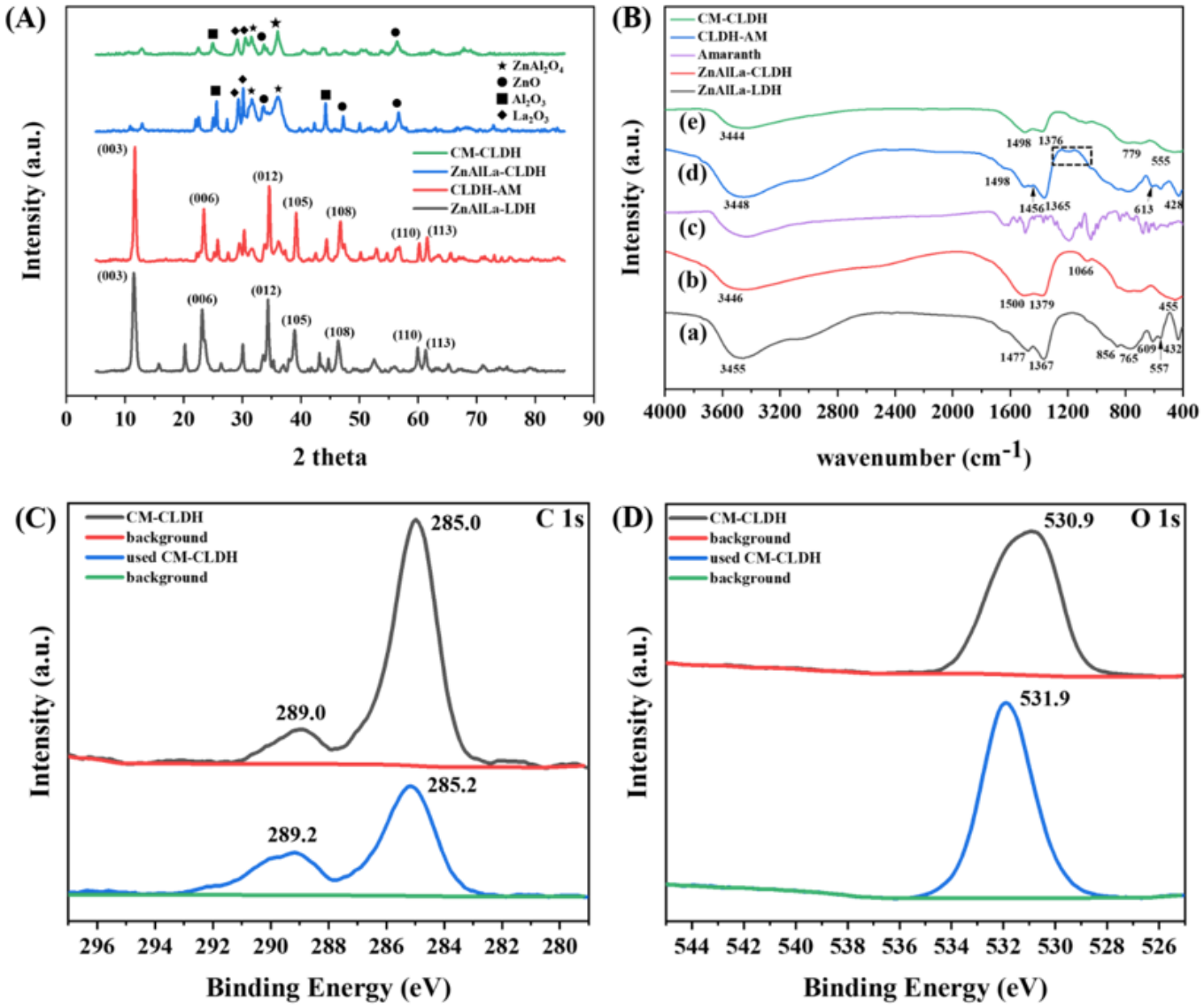

Figure 1

XRD patterns of prepared materials (A), FT-IR spectra of ZnAlLa-LDH (a), ZnAlLa-CLDH (b), amaranth (c), CLDH-AM (d), CM-CLDH (e) (B), XPS spectra of C 1s (C) and O 1s (D).

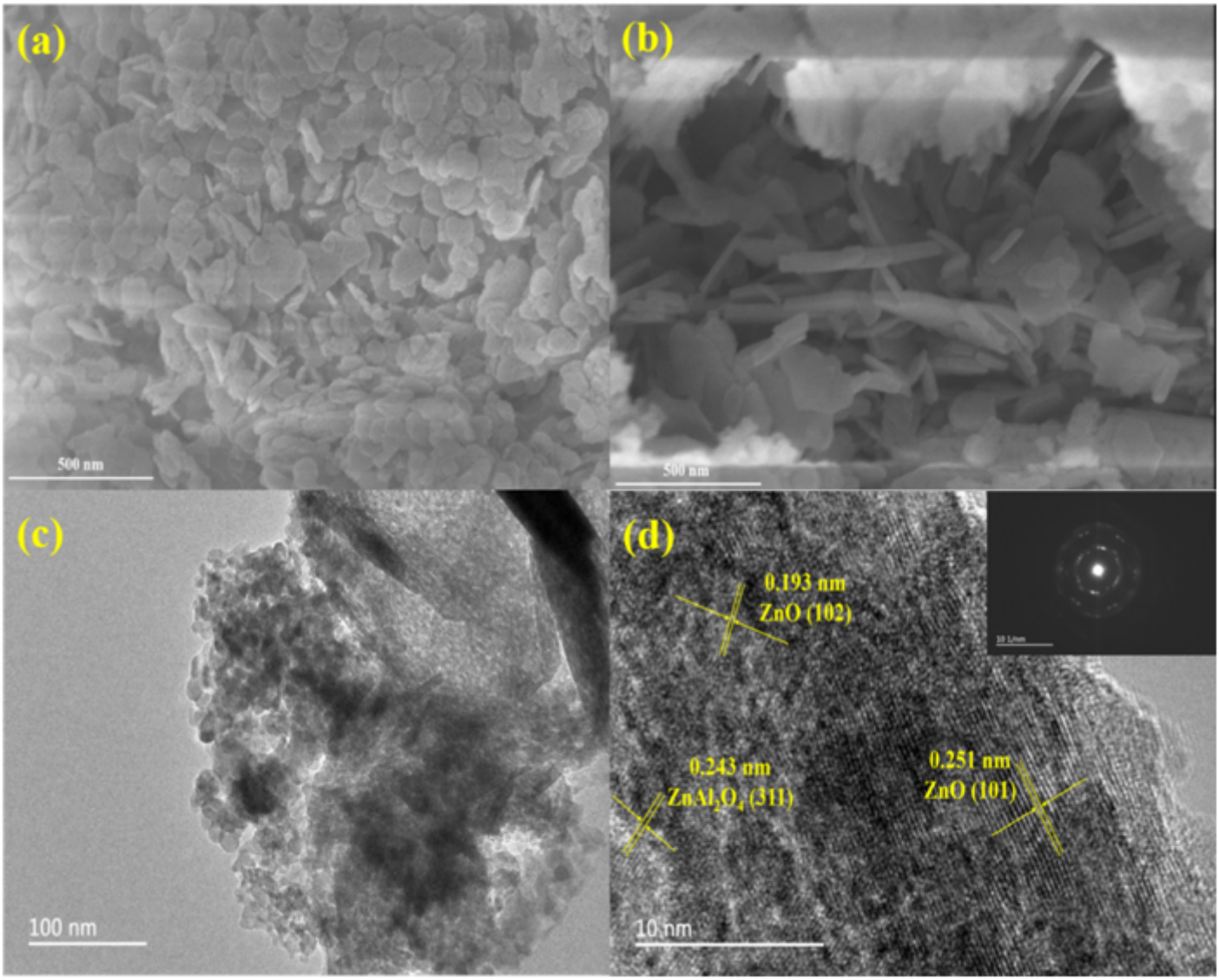

Figure 2

SEM images of ZnAlLa-CLDH (a), CM-CLDH (b), TEM image of CM-CLDH (c) and HRTEM image and SAED pattern of CM-CLDH (d)

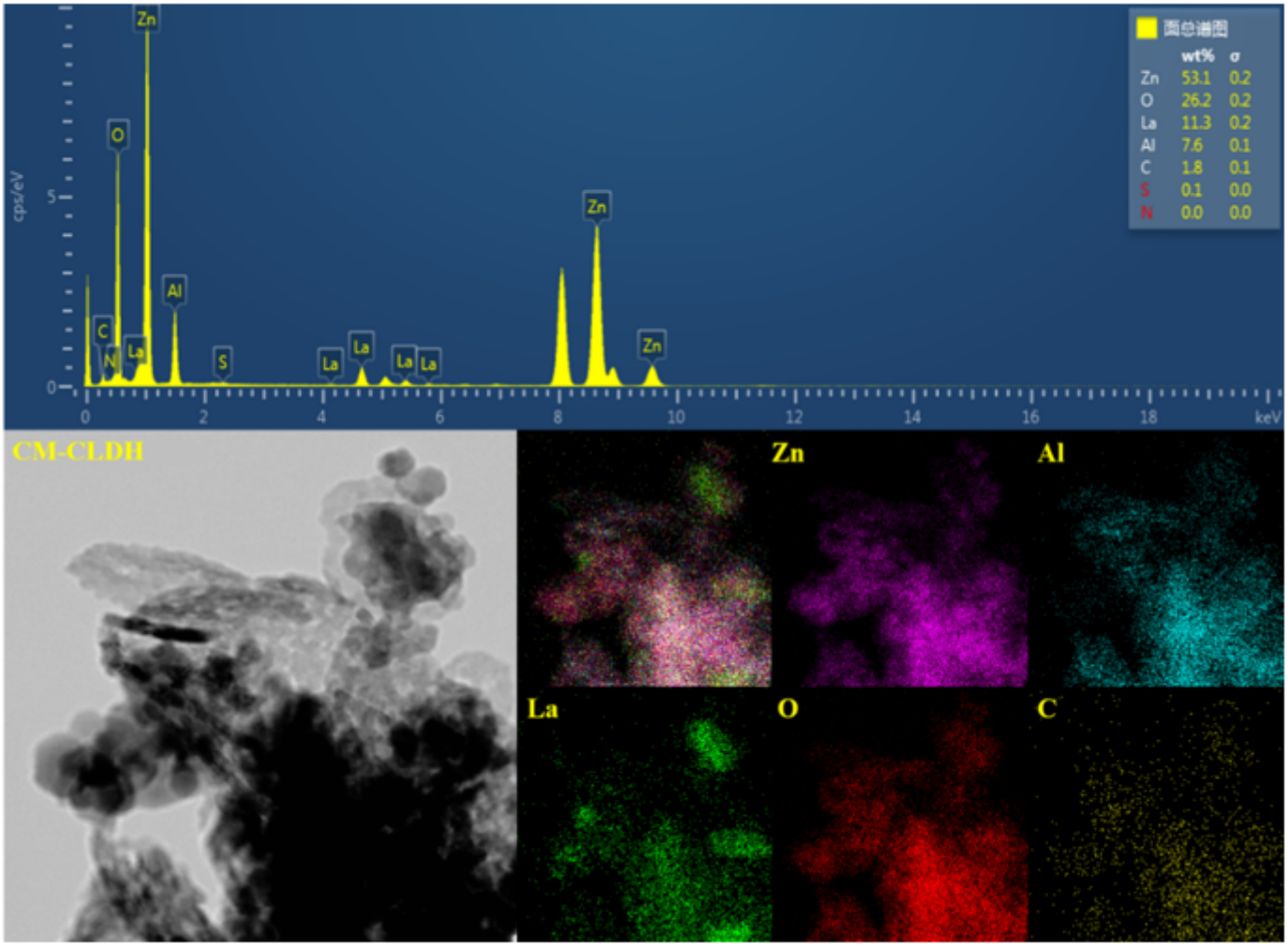

Figure 3

Elemental mapping analysis of CM-CLDH

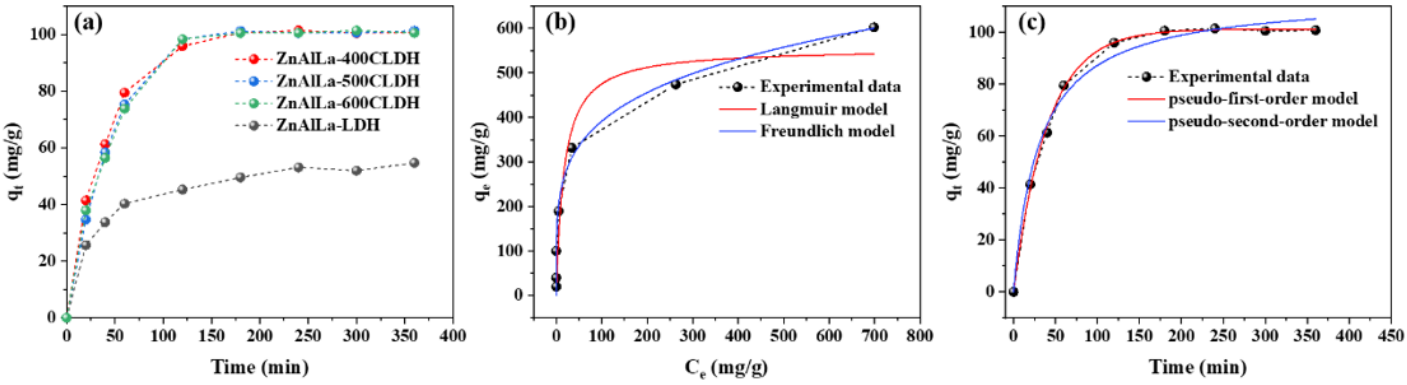

Figure 4

Adsorption of amaranth (50 mg/L) by LDH/CLDHs as a function of time (a), adsorption kinetics of amaranth on ZnAlLa-400CLDH (b), adsorption isotherm of amaranth on ZnAlLa-400CLDH (c).

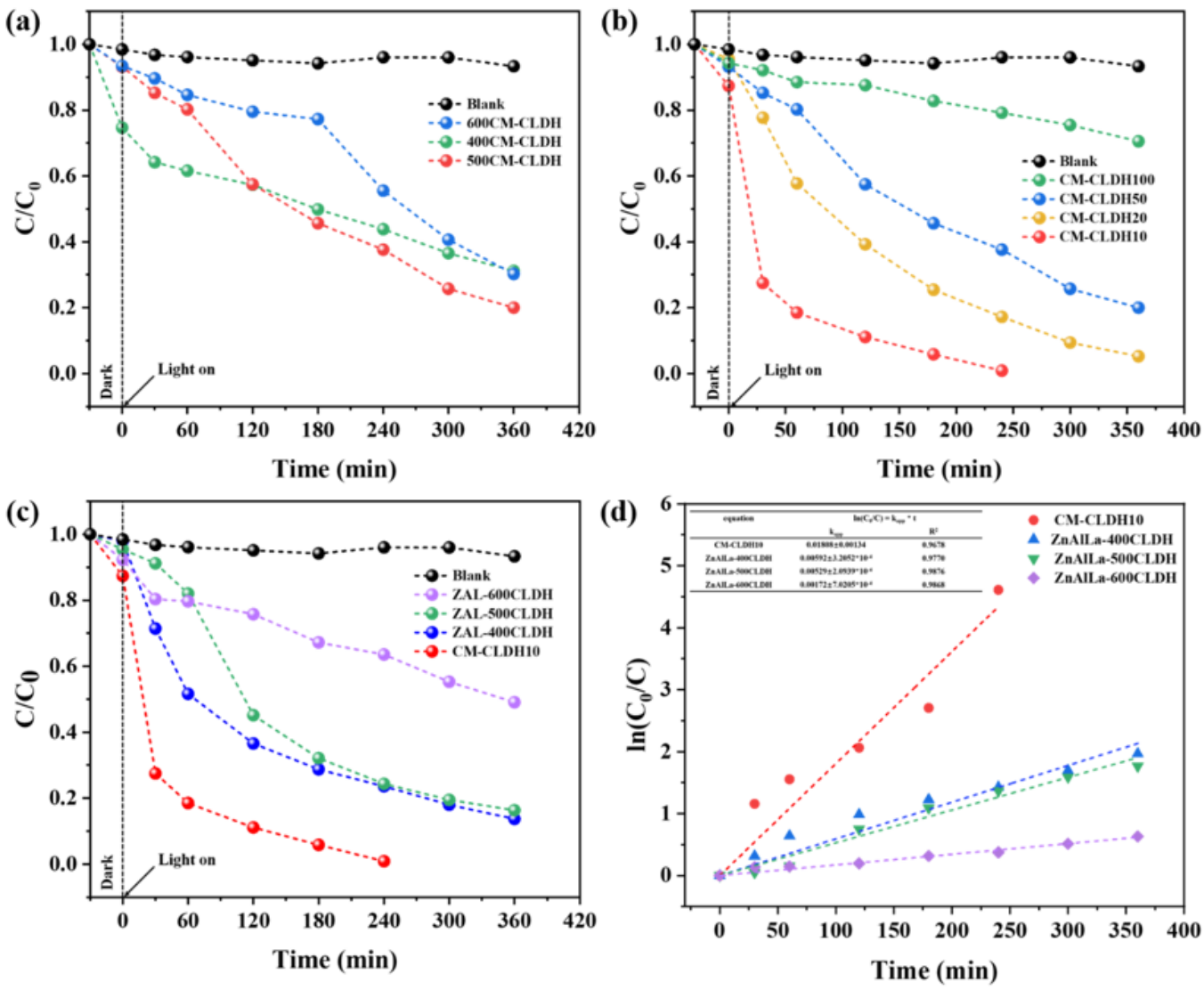

Figure 5

Photodegradation effeciencies of materials farbricated with different conditions: calcination temperature change on CLDH with the same amaranth adsorption amount (a), amaranth adsorption amount change on CLDH calcined 500 °C (b). Comparision between CM-CLDH10 and CLDHs calcined at different temperature (c), psuedo-first-orfer plot under simulate sunlight with different catalysts (d).

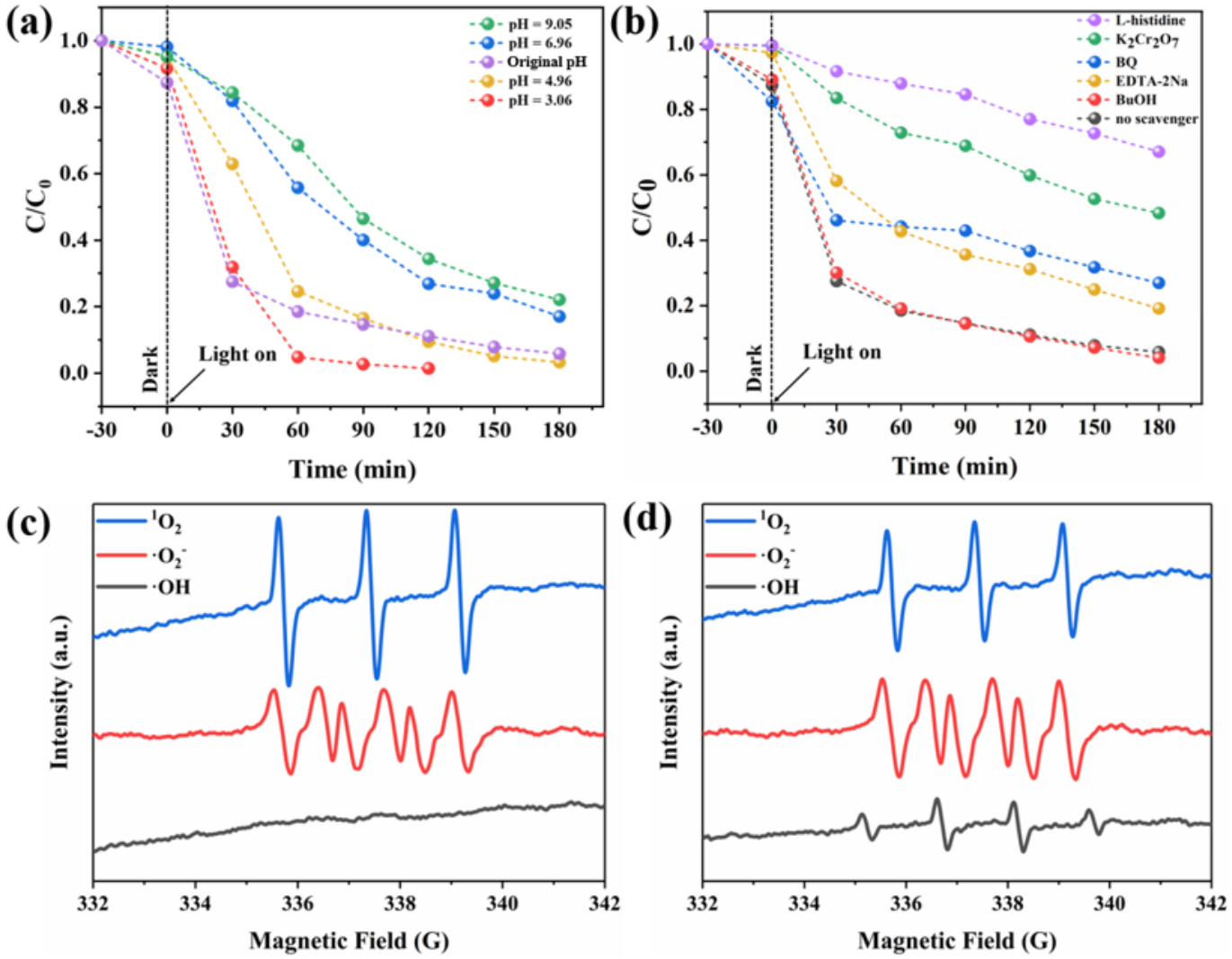

Figure 6

Photodegradation efficiency over CM-CLDH10 under different pH conditions (a), Photodegradation efficiency over CM-CLDH10 with existence of different radical scavengers. ESR signals of 1O2, ·O2- and ·OH over ZnAlLa-500CLDH (c) and CM-CLDH10 (d).

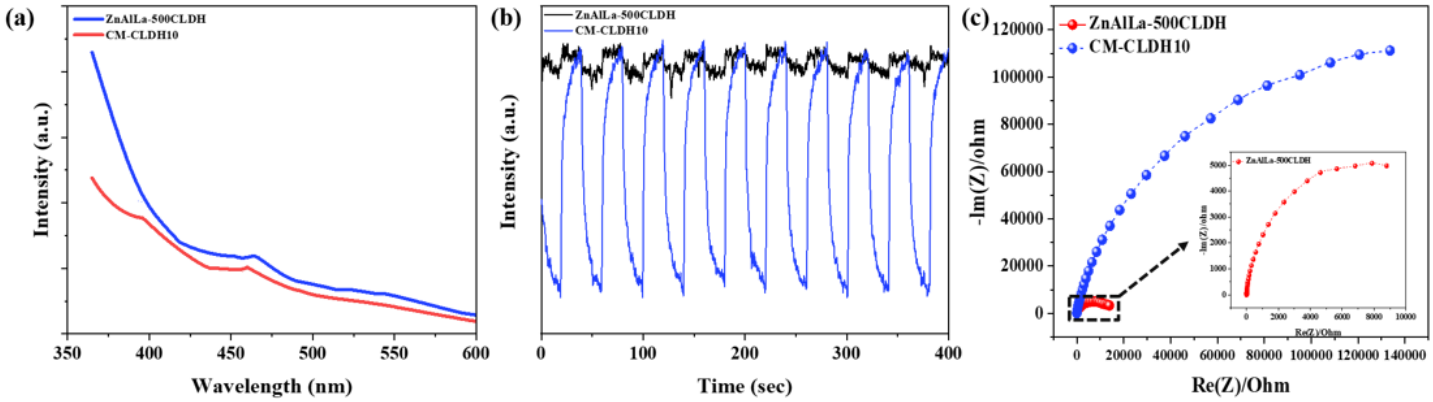

Figure 7

Photoluminescence (PL) spectra (a), photocurrent plot (b) and EIS Nyquist plot (c) of ZnAlLa-500CLDH and CM-CLDH10.

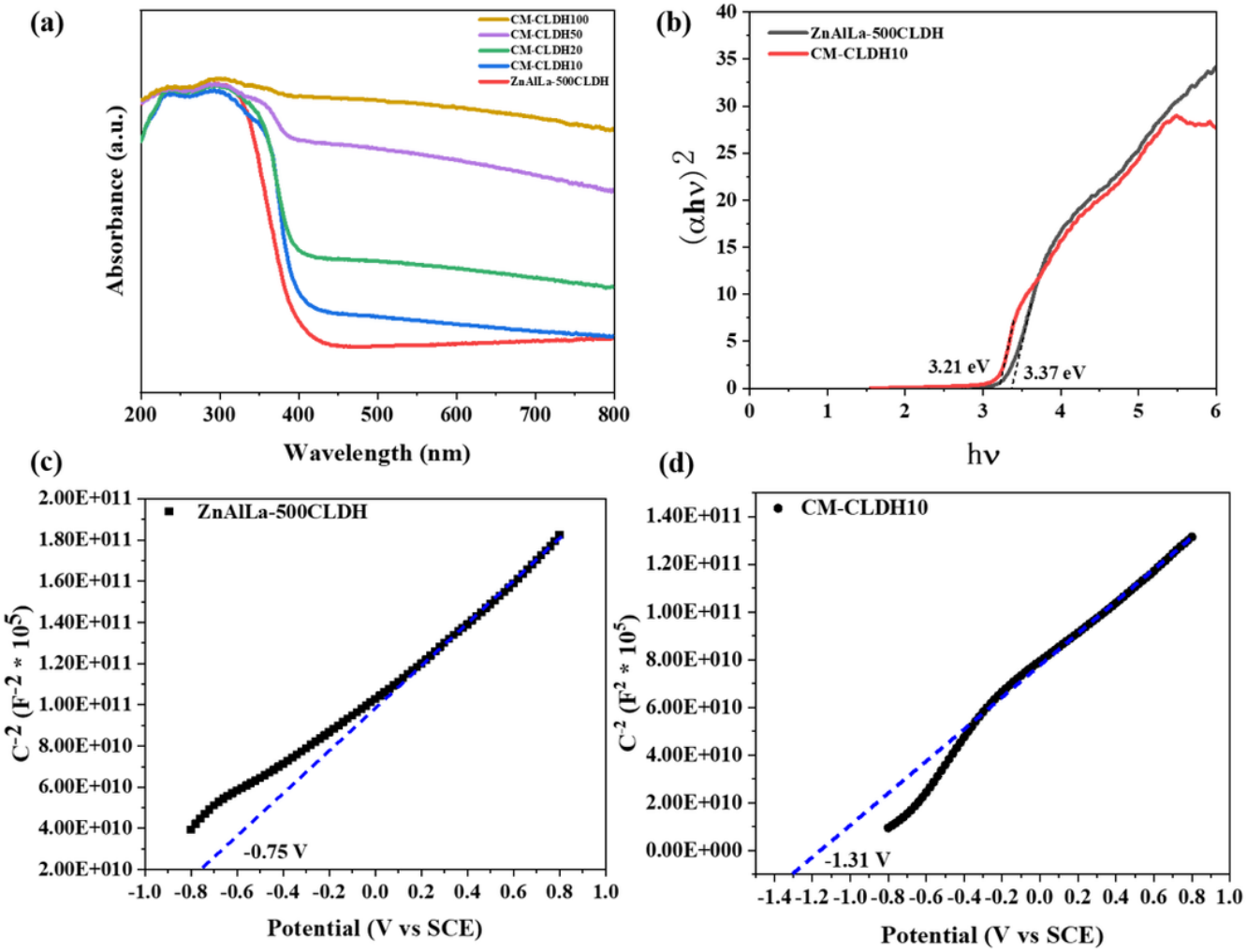

Figure 8

UV-vis/DRS plot of synthesized samples (a), corresponding Kubelka-Munk transformed reflectance spectra of ZnAlLa-500CLDH and CM-CLDH10 (b), Mott-Schottky plots of ZnAlLa-500CLDH (c) and CM-CLDH10 (d)

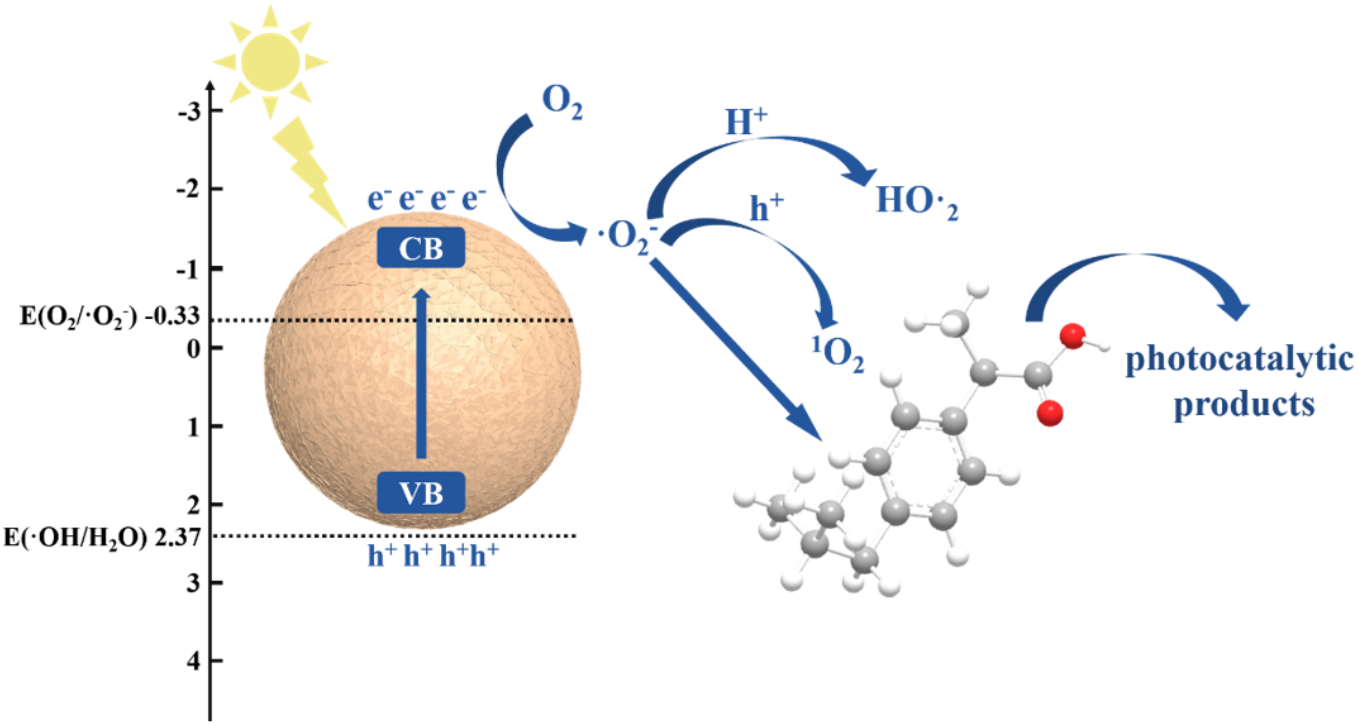

Figure 9

Schematic diagram of Ibuprofen photodegradation process over CM-CLDH10